Inorganica Chimica Acta 529 (2022) 120654

Contents lists available at ScienceDirect

Inorganica Chimica Acta

journal homepage: www.elsevier.com/locate/ica

Review article

A theoretical perspective on the reactivity of high-valent Mn-Oxo/nitrene species towards oxidative transformations

Asmita Sen, Ravi Kumar, Gopalan Rajaraman *

Department of Chemistry, Indian Institute of Technology Bombay, Mumbai 400076, India

A B S T R A C T

Metal-oxo species are ubiquitous in nature and play a pivotal role in various biological functions. While the popular Fe^{IV}=O/NTs species have been studied in detail over the years, equal undivided attention has not been paid to analogues Mn-oxo/nitrene species. Given the fact that some of the Mn-oxo/nitrene catalysts were found to be superior to their iron analogues, this necessitates the need to understand their intriguing reactivity pattern and how various factors such as spin-state, basicity, ligand architecture and oxidation state influence the reactivity. Various computational tools such as *ab initio* CASSCF and the Density Funtional Theory (DFT) calculations have been employed to understand mechanistic aspects related to the C—H and C═C bond activation of organic substrates. This minireview aims to cover theoretical aspects related to Mn-oxo/nitrene chemistry applied in various examples to illustrate how different their reactivity patterns are compared to the popular Fe^{IV}=O species.

1. Introduction

Aliphatic C—H bond functionalisation using earth-abundant metals as the catalyst is one of the top challenges in bio-mimic chemistry.[1] In this area, synthetic non-heme Fe^{IV}=O species, in particular, are proven to be very effective in various oxidative reactions such as substrate desaturation, hydroxylation or halogenation. Previous spectroscopic, kinetic and theoretical studies have revealed that the catalytic reactivity of these biomimic high-valent iron-oxo species is strongly regulated by involvement of various spin states, ligand architecture, ligands in the primary coordination sphere, which directly influence the basic properties such as p*K*a and redox potential of these species. For instance, the density functional theory (DFT) calculations established that the most synthetic Fe^{IV}-oxo species possess an S = 1 triplet spin as the ground state, but during the hydrogen atom transfer (HAT) from an unactivated C—H bond, a low-lying S = 2 quintet spin state comes into the picture to offer a comparatively lower barrier for the C—H bond activation, easing the kinetic barrier and often becoming the rate-determining step.[2–4] Thus, the role of the high-spin state in reducing the barrier heights of key oxidative organic transformations are unequivocally established. While various reasons for a lower kinetic barrier for the high-spin state compared to the low-spin states are proposed, the most intriguing explanation is based on the fact that a large number of unpaired electrons at the transition state facilitate the exchange of the same type of electron with the C—H bonds, offering large kinetic exchange stabilisation, which reduces the kinetic barrier dramatically. This phenomenon of utilising more unpaired electrons to reduce the energy barrier in a reaction is called exchange-enhanced reactivity or EER.[5,6,7,8] The concept of EER has been extensively used to explain reactivity trends in various species.[5]

Unlike high-valent Fe-oxo, their Mn-counterpart is less explored. Inspired by the reactivity of various metalloproteins in water oxidation, such as tetramanganese cluster of the oxygen-evolving complex (OEC) in photosystem II (PSII) and their ambiguous reactivity, several high-valent biomimic Mn-oxo species have been synthesised and characterised to date, though their reactivity was found to be sluggish and strongly substrate-dependent. Recently Nam and Jackson groups have shown that Mn^{IV}=O groups ligated to the neutral pentadentate N5-ligands are strongly oxidising, some cases even exceeding the reactivity of Fe-analogues.[9] Examples include $[(2pyN2Q)Mn^{IV}O]^{2+}$ and $[(BnTPEN)Mn^{IV}O]^{2+}$ complexes (Scheme 1, where 2pyN2Q and BnTPEN are 1,1-di(pyridin-2-yl)-*N*,*N*-bis(quinolin-2-ylmethyl)methanamine and *N*-benzyl-N,N',N'-tris(2-pyridylmethyl)ethane-1,2-diamine respectively) which can oxidise substrates with C—H bond dissociation energies of ~99 kcal/mol.[10] In line with this, Nam and co-workers have observed an enhancement of reactivity of the Mn^{IV}=O species in the presence of strong Bronsted acids such as lewis acid Sc^{III}, triflic acid etc.[11] Moreover, Jackson and Borovik group proposed that the high reactivity of these Mn-oxo complexes is connected to the very high Mn^{IV}/Mn^{III} one-electron standard reduction potential as well as on the basicity of the oxo groups.[12–14] These proposals lead to several possibilities, but a concrete understanding of the origin of the reactivity

* Corresponding author.
E-mail address: rajaraman@chem.iitb.ac.in (G. Rajaraman).

https://doi.org/10.1016/j.ica.2021.120654
Received 20 August 2021; Received in revised form 30 September 2021; Accepted 4 October 2021
Available online 8 October 2021

remained unavailable, providing various open questions in this area. Although the reactivity pattern, as well as the parameters controlling the reactivity of the analogous Fe-oxo complexes, are well-established and summarised in several reviews,[6,15–17] the chemistry of Mn-oxo species is not documented/reviewed.

Apart from Mn-oxo species, analogues Mn-nitrene species also gained attention because of the higher reactivity of Fe^{IV}=NTs species reported for some analogues compared to their Fe^{IV}=O counterparts.[18,19] The Mn-nitrene species have the capability to perform reactions such as C—H amination[20] and aziridination[21] with high stereo- and regio-specificity. In addition, aziridine and amine moieties are present in the natural products and show biological activities, making them pharmaceutically important moieties.[22–28,21] To compare and contrast the reactivity of Mn-oxo species with Mn-nitrenes, we have also reviewed the relevant literature to understand their comparative oxidative abilities.

This minireview aims to summarise the role of theoretical studies, including DFT and *ab initio* methods, in understanding the mechanistic insights into the reaction catalysed by high-valent Mn-oxo and Mn-nitrene species. Particularly the reactivity of Mn^{III}=O, Mn^{IV}=O and Mn-nitrene in C—H/C═C bond activation containing various ligand architecture (Scheme 1) and how important the concept of two-state reactivity in rationalising the reactivity of these species are highlighted.

2. Mechanistic insights on non-heme High-valent Mn-Oxo species

2.1. Six-coordinated Mn^{IV}=O species

The intriguing reactivity pattern of *hexa*-coordinated high-valent Mn-oxo complexes has been documented by Cho et al. [29] for the first time while exploring the reactivity of two non-heme Mn^{IV}=O species, namely, $[(Bn\text{-}TPEN)Mn^{IV}O]^{2+}$ (**2**) and $[(N4Py)Mn^{IV}O]^{2+}$ (**3**) (where N4Py is N,*N*-bis(2-pyridylmethyl)-*N*-bis(2-pyridyl)methylamine; Scheme 1) with cyclohexane as substrate. Involvement of richer electronic participation is observed for Mn^{IV}=O species as compared to their Fe-analogues. In most of the complexes, the $S = {}^3/_2$ spin state is found to be the ground state, which remains unaltered during the course of the reaction, ruling out the possibility of other spin states involvement.

Like Fe^{IV}=O, conventional two-state reactivity is not operative in Mn^{IV}=O chemistry; instead, a more complex excited-state reactivity is found to be operational. Calculations show that the hydrogen atom transfer catalysed by these complexes begins with the $^4B_1$ state as the ground state. This state is arising from $b_2(\delta)^1\, e(\pi^*_{xz}, \pi^*_{yz})^2$ configuration (C_{4v} symmetry label). In the C—H activation transition state, a high-lying ^4E state (40.7 kJ/mol, for ***2***), arising from a transfer of an electron from occupied $e(\pi^*_{xz}, \pi^*_{yz})$ to the unoccupied $b_1(\sigma^*_{xy})$ orbital, becomes ground state compared to the $^4B_1$ state at the reactant level and this lowering of the excited state of same spin multiplicity found to be responsible for their high-reactivity (54.6 kJ/mol vs 115.1 kJ/mol, for 2) (Fig. 1a). The presence of excited states in $[(N4Py)Fe^{IV}O]^{2+}$ species were found to exhibit photochemical reactivity with the excitation around 14367 cm^{-1} for C—H bond activation of DHA.[30] These excited states are accessible via electronic absorption in the near-infrared (IR) region. Jackson and co-workers by employing electronic absorption and variable-temperature magnetic circular dichroism (MCD) spectroscopy have shown that $[(N4Py)Mn^{IV}O]^{2+}$ species has a characteristic feature in the near-IR region (~10500 cm^{-1}), which is related to the d_{xz} to $d_{x^2-y^2}$ excitation.[31] The possibility of using such excitation to effect organic transformation in Mn-oxo chemistry is thus very appealing. The rate enhancement in the singly excited ^4E state is proposed to be due to the exchange enhance reactivity (EER) in the corresponding transition state. These $e(\pi^*_{xz}, \pi^*_{yz})$ orbitals were strongly antibonding to the Mn=O unit; therefore, electron transfer from these orbitals can affect the Mn-O bond parameters and alter the Mn^{III}-oxyl radical characters. Fig. 1c demonstrates the transfer of different spins from the $\sigma_{C\text{-}H}$ bond to Mn d-orbitals. It reveals that in the lowest energy transition state, a spin-up α-electron is transferred to the vacant π^*_{xz} orbital, and this avoids an additional energy penalty for the spin relaxation which is present in the high-lying $^4B_1$ transition state. In the $^4B_1$ case, a spin-down β-electron is transferred to a higher energy (π^*_{xz}) orbital while the lower energy (δ) orbital is singly occupied. The enhancement of the spin-orbit coupling in the intermediate generated via the excited state also facilitates reactivity. Later, the Mn^{III}-OH intermediate is found to undergo a dissociative

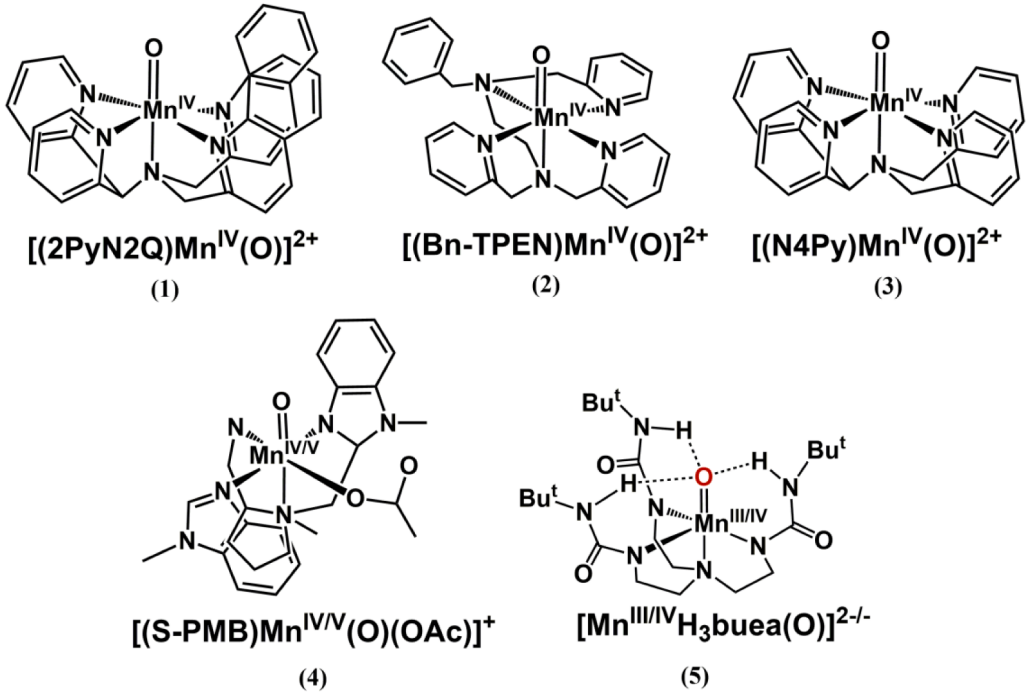

Scheme 1. Schematic drawing of the chemical structures of $[(2PyN2Q)Mn^{IV}O]^{2+}$ (**1**) $[(Bn\text{-}TPEN)Mn^{IV}O]^{2+}$ (**2**), $[(N4Py)Mn^{IV}O]^{2+}$ (**3**), $[(S\text{-}PMB)Mn^{IV/V}(O)(OAc)]^{2+}$ (**4**) and $[Mn^{III/IV}(O)H_3buea]^{2-/-}$ (**5**).

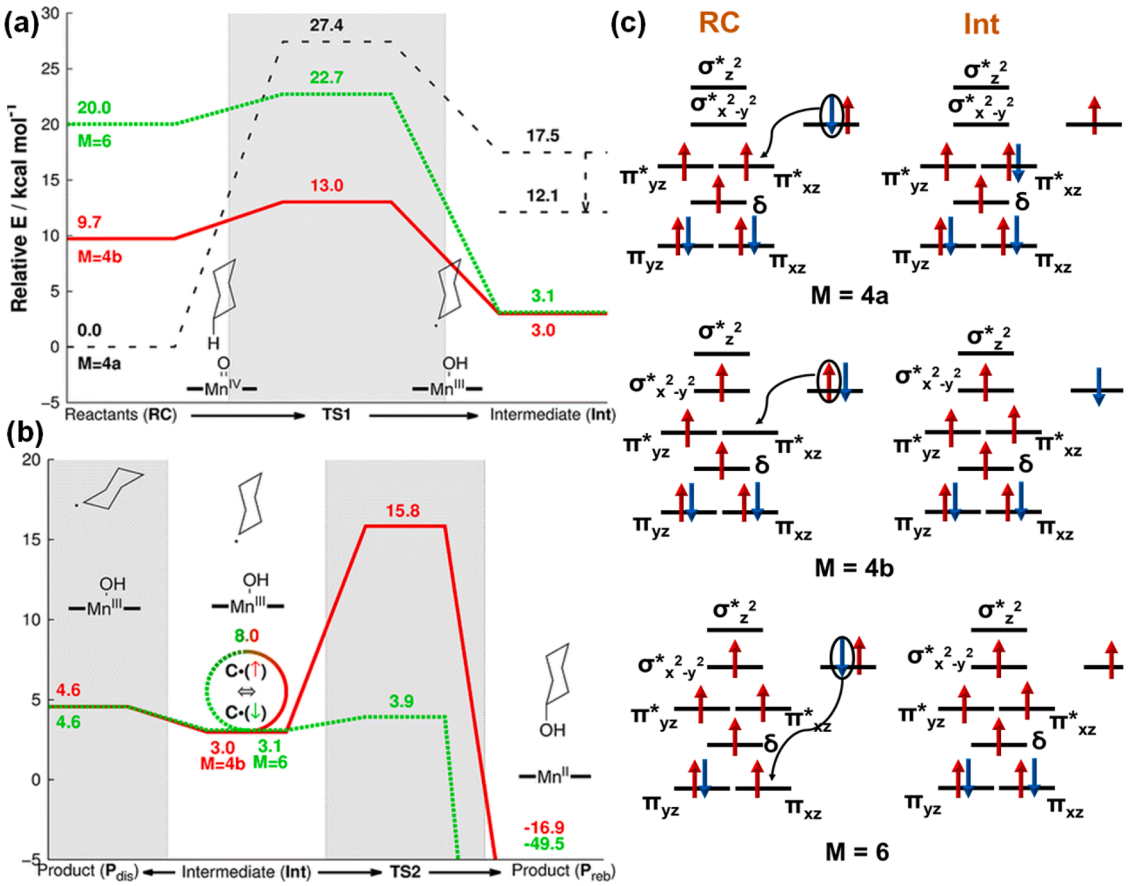

Fig. 1. (a) and (b) are the energy profile for the initial C—H bond activation step (rate-determining) in the reaction of 1 and cyclohexane and dissociation vs. rebound reaction energies for the same. (c) Electron shift diagram between the Mn d-orbital and σ_{CH} orbital during the C—H activation step. Blue indicates an α-electron transfer, whereas the red indicates a β-electron transfer from ref. 29 Copyright (2012) American Chemical Society.

pathway (19.3 kJ/mol) over desaturation and –OH rebound mechanism (33.6 kJ/mol). Although the exchange interaction was found to be similar for the Mn^{III}-OH intermediate generated from S = $^3/_2$ excited state pathway and S = $^5/_2$ surface (only differ in their spin orientation on the carbon centre), the involvement of the high-spin state is eliminated owing to the additional energy required for the spin-flip, resulting in the barrier which is higher than the dissociative pathway (Fig. 1b).

After Nam and Shaik, Jackson and co-workers have evaluated the electronic excitation of $[(N4Py)Mn^{IV}O]^{2+}$ species using electronic absorption and magnetic circular dichroism spectroscopy and assigned a low energy feature at near-IR region (TD-DFT = 12700 cm^{-1}, experimental = 10500 cm^{-1}) associated with the (d_{xz}, d_{yz}) to $d_{x^2-y^2}$ transition (^4E) (Fig. 2a and b).[31] Moreover, they have investigated the configurational changes in $[(N4Py)Mn^{IV}O]^{2+}$ as a function of Mn=O bond length employing the *ab initio* CASSCF/NEVPT2 method. Calculations reveal that at the equilibrium Mn-O bond distance, the electronic configuration of the ground $^4B_1$ state is dominated by $(p_z)^2$ $(p_x)^2$ $(p_y)^2$ $(d_{xy})^1$ $(d_{xz})^1$ $(d_{yz})^1$ configuration with a negligible contribution from the Mn^{III}-oxyl species (S = 1 spin in Mn^{III} ferromagnetically coupled with the S = $^1/_2$ spin on oxyl radical). The Mn^{III}-oxyl radical species contribution $[(p_z)^2$ $(p_x\ p_y)^3$ $(d_{xy})^1$ $(d_{xz})^1$ $(d_{yz})^1$ $(d_{x^2-y^2})^1]$ to the formal Mn^{IV}=O species, on the other hand, is found to be relatively higher (15%) in the high-lying ^4E state. The elongation of the Mn-O bond in the $^4B_1$ state, though it alters the overall energy, the ground state electronic configuration detected is unaltered throughout. Further, the Mn^{III}-oxyl character remains negligible throughout, suggesting that this state is truly Mn^{IV}=O species, irrespective of the Mn-O bond lengths.

In contrast, with Mn-O bond elongation, the % of oxyl radical character in ^4E surface is found to increase gradually, and beyond the C—H bond activation transition state, Mn^{III}-oxyl(π) radical species is found to be dominating. From these observations, it has been made clear that a steady increase in the Mn^{III}-oxyl radical character in the ^4E surface during the course of the reaction is predominantly responsible for the enhanced reactivity. Apart from the Mn-oxyl character, another driving force is found to be operating here. A transfer of spin-down β-electron from the σ_{CH} orbital to the partially filled d_{xz}/d_{yz} orbital in $^4B_1$ results in the spin pairing, diminishing the number of kinetic exchange and formation of less stable Mn^{III}-intermediate, which requires a spin relaxation for further stabilisation. This spin-pairing penalty is avoided in the ^4E state, where both Mn^{IV}=O and Mn^{III}-oxyl(π) species are generating a stable Mn^{III} intermediate via a respective α and β-electron transfer to the d_{xz}/d_{yz} and $p_{x/y}$ orbital leading to a $(p_z)^2$ $(p_x)^2$ $(p_y)^2$ $(d_{xy})^1$ $(d_{xz})^1$ $(d_{yz})^1$ $(d_{x^2-y^2})^1$ configuration. Therefore, besides the developing oxyl character, the stability of the Mn^{III}-intermediate also plays a crucial role in controlling the reactivity. In a tetragonal environment the C—H activation rate of the $[Mn^{IV}(O)(BnTPEN)]^{2+}$, $[Mn^{IV}(O)(N4py)]^{2+}$, and $[Mn(O)(OH)(Me_2EBC)]^+$ species are found to be $[Mn^{IV}(O)(BnTPEN)]^{2+}$ > $[Mn^{IV}(O)(N4py)]^{2+}$ > $[Mn(O)(OH)(Me_2EBC)]^+$.

Further, Rice et al. have shown that both DFT and *ab-initio* CASSCF/NEVPT2 calculations on the HAT reactions of ethylbenzene catalysed by $[Mn^{IV}O(N4Py)]^{2+}$ species agree with the involvement of multiple electronic states of the same multiplicity ($^4B_1$ and ^4E) during the reaction.[32] Although the B3LYP-D3 methodology underestimates the activation energy barrier for the $^4B_1$ and ^4E states, both methods support the presence of the multireference character in dictating the reactivity. The origin of the difference in the $^4B_1$ and ^4E transition states has again been identified. It is found that while the $^4B_1$ state is predominantly an S = $^3/_2$ Mn^{IV}=O species with a negligible contribution from the Mn^{III}-$O^{\bullet}$ species,

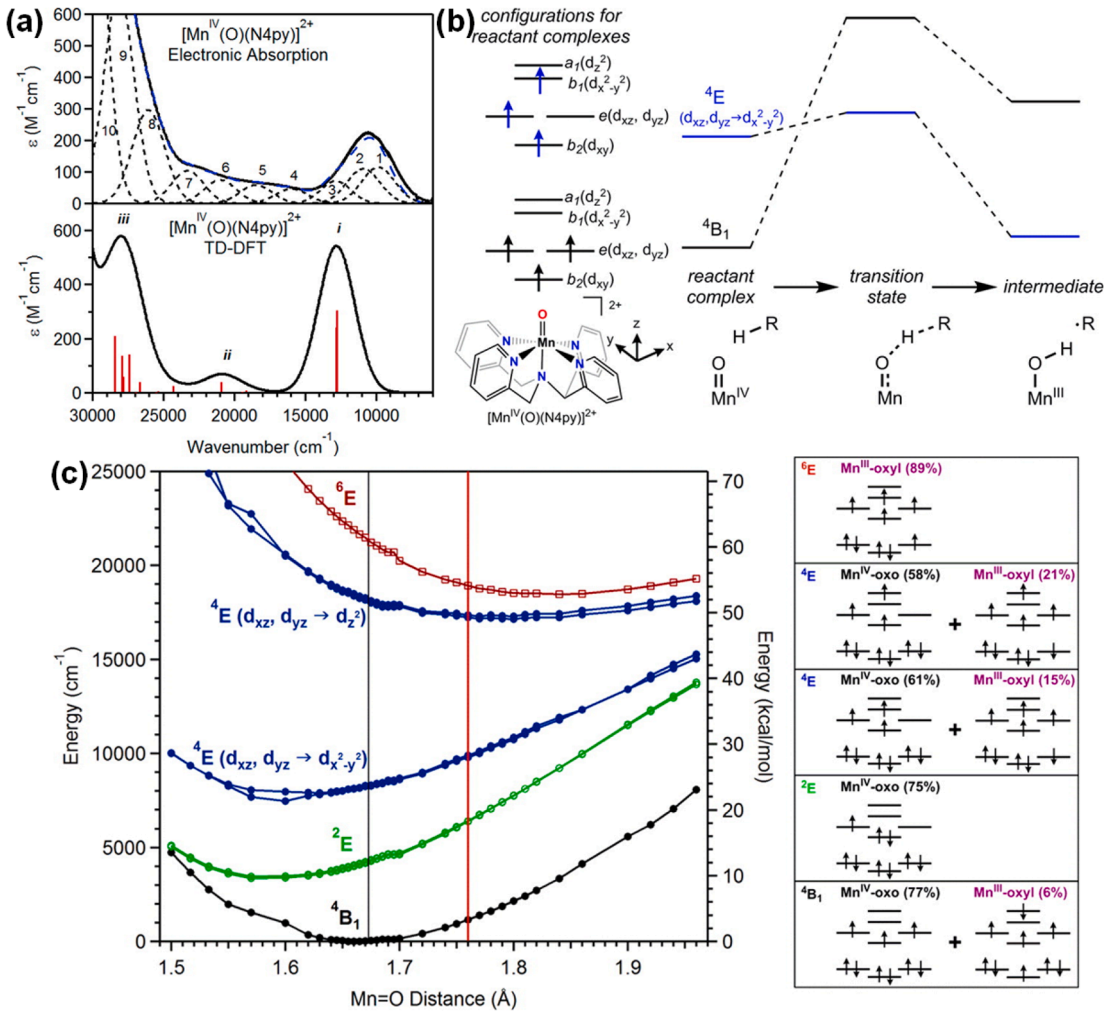

Fig. 2. (a) Experimental and TD-DFT-calculated electronic absorption spectrum of $[Mn^{IV}(O)(N4py)]^{2+}$ (black and blue traces are individual Gaussian curves and their sums, red sticks represent individual electronic transitions), (b) ground State ($^4B_1$) and lowest-lying quartet excited state (^4E) in the reaction coordinates during the HAT reaction, (c) CASSCF/NEVPT2 calculated potential energy surfaces of the lowest-energy states of $[Mn^{IV}(O)(N4py)]^{2+}$ as a function of the Mn-O distance from ref. 31 Copyright (2016) American Chemical Society.

a sufficiently large contribution from Mn^{III}-O$^{\bullet}$ species is originated in the ^4E state. The $(\sigma_z)^2$ $(\pi_1)^2$ $(\pi_2)^2$ $(d_{xy})^1$ $(\pi_1^*)^1$ $(\pi_2^*)^1$ (σ_{eq}^*) (σ_z^*) configuration is found to be contributing 89% to the total wave function in the $^4B_1$ transition state, whereas, the ^4E transition state is composed of the 64% contribution from a state generated by $\pi_1^* \rightarrow \sigma_{eq}^*$ transition and 13% contribution is arising from a $\pi_1(O) \rightarrow \pi_1^*(M)$ excitation. Due to the electron donation to the antibonding π_1^* orbital of the M=O unit, the M=O bond order decreases in the ^4E transition state with a higher oxyl radical character. Apart from mixing the ground state with the excited state configuration in the ^4E transition state, the spin polarised nature of Mn and oxyl radical results in the maximum orbital overlap involving the electron-donating σ_{CH} orbital and the electron-accepting π^* antibonding M=O orbital. The ^4E state is easily accessible due to the flexible equatorial ligands of N4py, which undergo elongation to enable access to the excited states. Although the distortion is energetically expensive, the favourable substrate-catalyst interactions can easily compensate for this energy penalty, facilitating the reaction via an excited state. Chen and Cho et al. further found that the $[Fe^{IV}O(N4Py)]^{2+}$ species is more reactive than $[Mn^{IV}O(N4Py)]^{2+}$ towards the hydrogen atom transfer (HAT) as well as oxygen atom transfer (OAT) reactions in an identical reaction condition and also confirms the excited state reactivity for the later. [33] An $S = {}^3/_2$ state is found to be as the ground state for $[Mn^{IV}O(N4Py)]^{2+}$ species. Both HAT (substrate: 1,4-cyclohexadiene, CHD) and OAT (substrate: *para*-X-thioanisole derivatives where, X = MeO, Me, H, F, and Br) reactions are occurring via an excited state reactivity (64.2 kJ/mol and 39.06 kJ/mol respectively) where an electron excitation from π^*_{yz} to σ^*_{xy} orbital is taking place followed by the transfer of spin up α-electron to a metal π^*_{yz} orbital from the substrate. The reactivity was found to occur via π-channel for both cases involving α-electron transfer. In the case of HAT, the other two possible channels are (i) α-electron transfer to the $\sigma_z{}^{2*}$ leading to a σ-channel (86.1 kJ/mol) and (ii) a β-electron is transferred to the π^*_{yz} orbital leading to another π-pathway (82.7 kJ/mol). Both of which are found to be higher in energy (Fig. 3). A similar kind of reactivity is found in $[(S\text{-}PMB)Mn^{IV}(O)(OAc)]^+$ (Scheme 1–4) species towards the C—H bond activation of cyclohexane studied by Li et al. [34] In support of the previous studies, the author has shown that only a single quartet $S = {}^3/_2$ state is found for the free catalyst, whereas another quartet state is found in the presence of substrate. The former one has an electronic configuration of $(\pi^*_{xy})^1$ $(\pi^*_{yz})^1$ $(\pi^*_{xz})^1$ $(\sigma^*_{x^2-y^2})^0$ $(\sigma^*_{z^2})^0$ $(^4B_1)$ while the latter reactant complex has $(\pi^*_{xy})^1$ $(\pi^*_{yz})^1$ $(\pi^*_{xz})^0$ $(\sigma^*_{x^2-y^2})^1$ $(\sigma^*_{z^2})^0$ (^4E) configuration. The ground $^4B_1$ state is found to be energy-demanding (131.8 kJ/mol) due to the transfer of a spin-down β-spin electron to the partially occupied π^*_{yz} orbital, hence facing spin-pairing energy penalty, which is not present in the $\pi^*_{xz} \rightarrow \sigma^*_{x^2-y^2}$ excited state resulting in higher reactivity (81.1 kJ/mol).

Comba and Sastri have synthesised, characterised and studied the reactivity of two non-heme mononuclear Mn^{IV}=O complexes with two

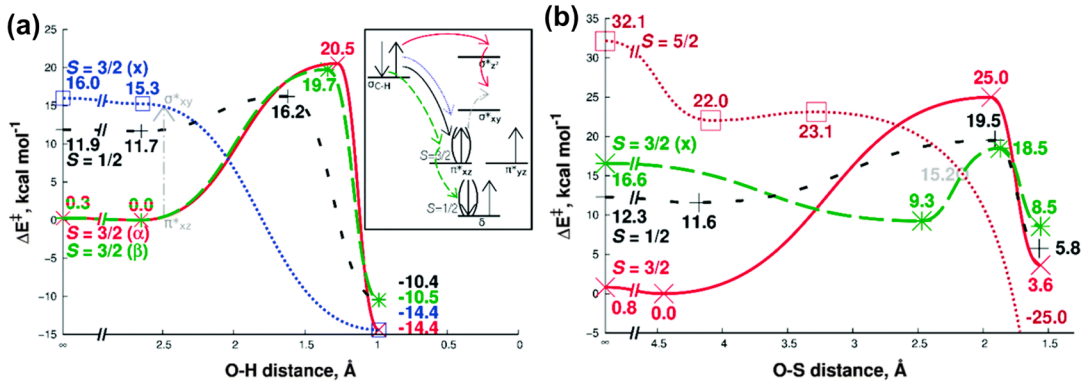

Fig. 3. Reaction energy profile for the (a) HAT and (b) thioanisole sulfoxidation reaction by 2 from ref. 33 Copyright (2015) The Royal Society of Chemistry.

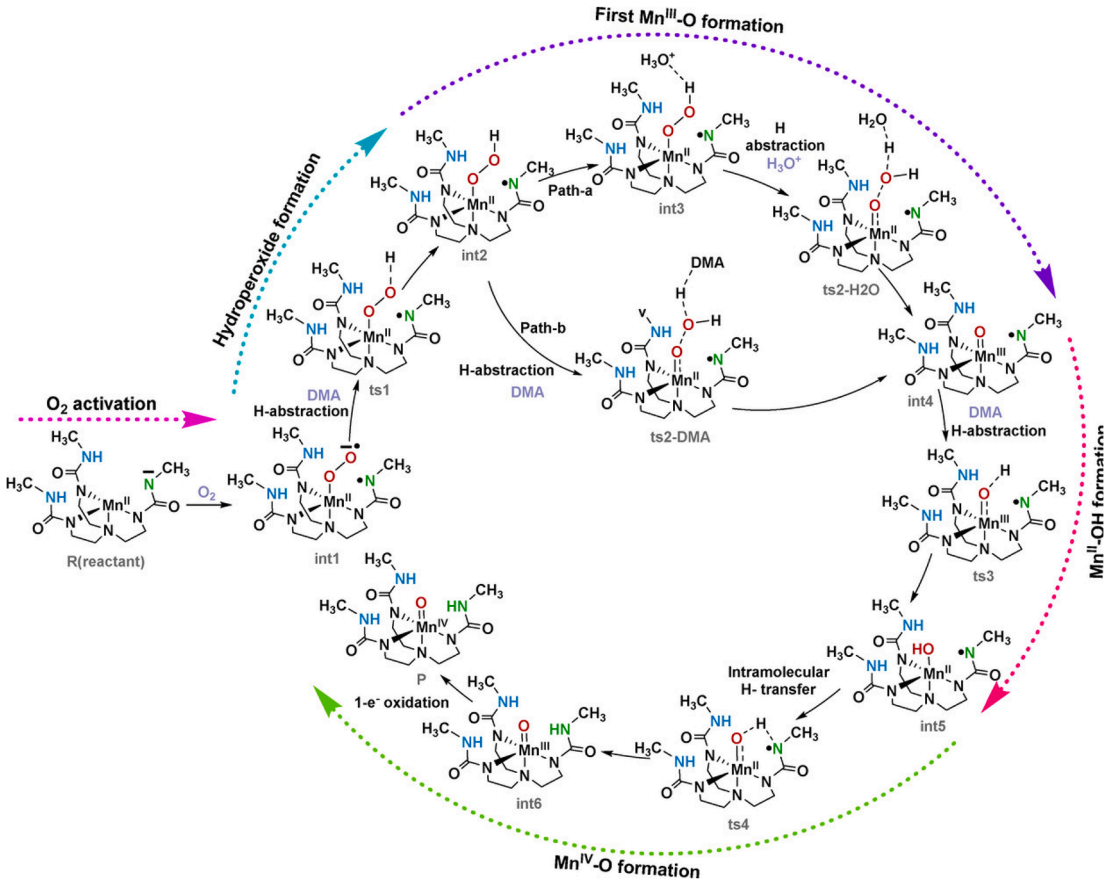

Scheme 2. Schematic diagram for the formation of $Mn^{III/IV}$ = oxo species from $[Mn^{II}H_2buea]^{2-}$. Here, DMA stands for dimethylacetamide which is used as solvent here. Reprinted (adapted) with permission from ref 38. Copyright (2020) Wiley-VCH Verlag GmbH & Co. KGaA, Weinheim.

isomeric bispidine ligands using both experiments and DFT methods. [35] The bispidine moiety has a rigid adamantane-derived structure and can exist in two isomeric (in N3 and N7 form) forms for the pentadentate ligands (Fig. 4). This exists in a square pyramidal geometry where the oxo-ligand is trans to N3 and N7 for L^1 and L^2. These two isomers show different reactivity as N7 is a part of a flexible 6-membered ring while the N3 is connected to a rigid five-membered ring. Experimentally it is found that the catalysts are following a HAT pathway, and $[Mn^{IV}(O)L^1]^{2+}$ is found to be more reactive than $[Mn^{IV}(O)L^2]^{2+}$ towards HAT as well as sulphoxidation reactions of thioethers. The reactivity pattern of Mn^{IV}=O isomers are different from their Fe^{IV}=O analogues, where $[Fe^{IV}(O)L^2]^{2+}$ is found to be more reactive than $[Fe^{IV}(O)L^1]^{2+}$. DFT calculations have been performed to understand these intriguing reactivity patterns and found that both isomeric Fe^{IV}=O species react via two-state reactivity starting with an S = 1 triplet state as the ground state and reacting via an S = 2 quintet state through a σ-channel. Similar to the previous studies, in the bispidine ligand environment (L^1 and L^2), Mn^{IV}=O species possess an S = $^3/_2$ high-spin state as the ground state and react via an S = $^1/_2$ surface following a π-pathway. In this study, a two-state reactivity of high-valent Mn-oxo species has been reported. The calculated energy barriers are estimated to be 44 kJ/mol, 33 kJ/mol, 71 kJ/mol and 65 kJ/mol for the $[Fe^{IV}(O)L^1]^{2+}$, $[Fe^{IV}(O)L^2]^{2+}$, $[Mn^{IV}(O)L^1]^{2+}$ and $[Mn^{IV}(O)L^2]^{2+}$ species respectively, therefore observing ambiguity in the Mn-species reactivity through the DFT study. Further, molecular mechanics analysis suggests that the L^1-based system has a higher molecular surface than the L^2-based one, making the metal-

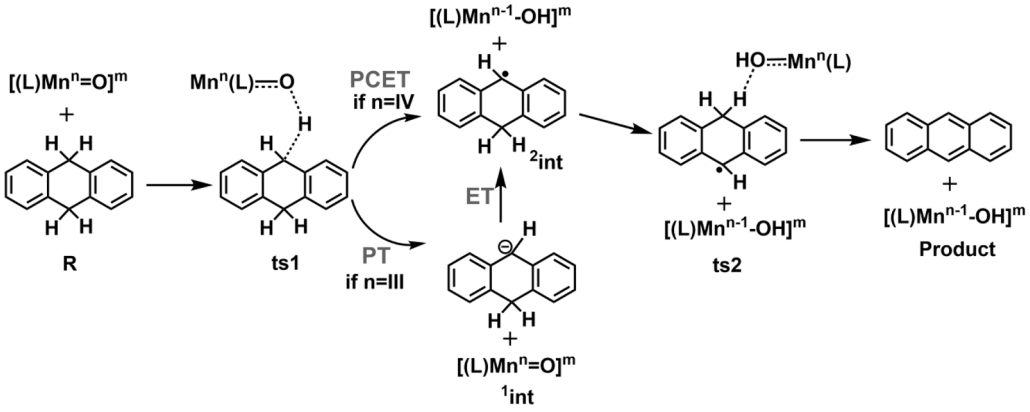

Scheme 3. Mechanistic scheme adopted for C—H activation reaction involving monomeric [(H_3buea)$Mn^{III/IV}$=O] complexes ref. 40 Copyright (2013) The Royal Society of Chemistry.

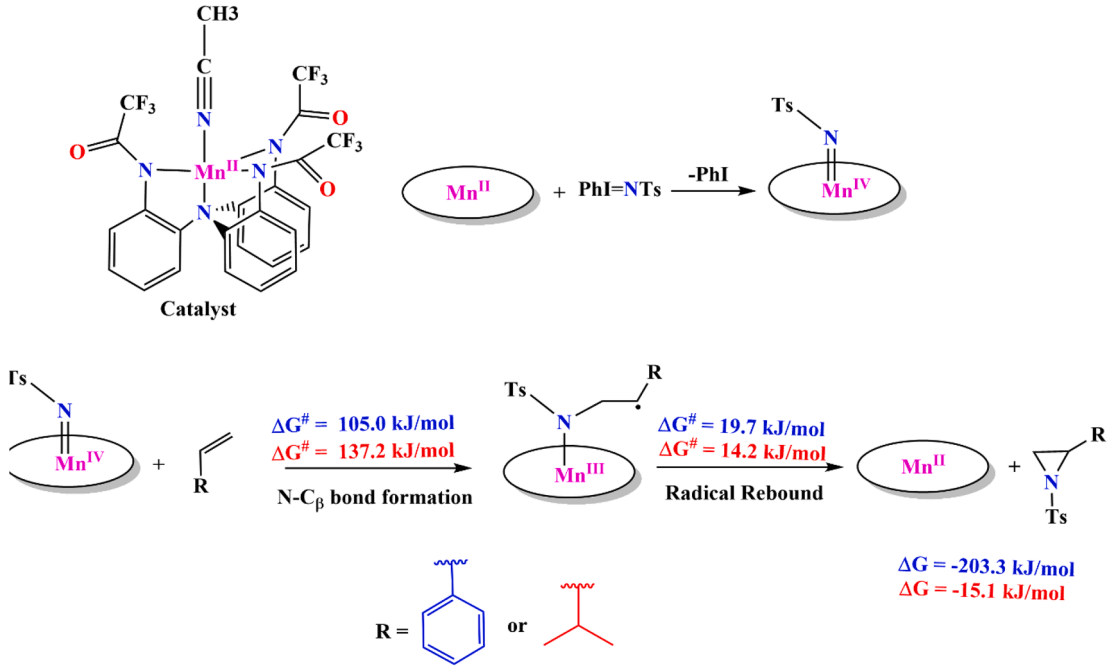

Scheme 4. Schematic representation of various pathways involved in the reaction with their activation barriers ($\Delta G^{\#}$) in kJ/mol from ref. [44].

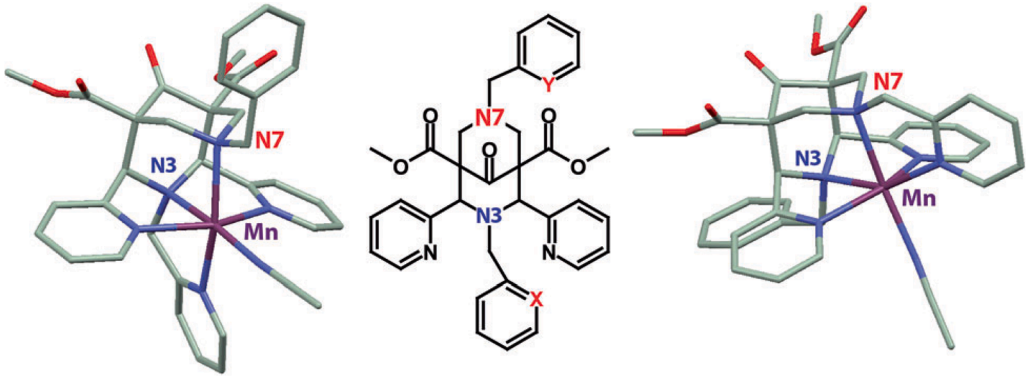

Fig. 4. Plots of the X-ray structures of [Mn^{II}(MeCN)(L^1)] (left (1), methylpyridine at N3, X = N, Y = CH, see drawing in the middle for X, Y), and [Mn^{II}(MeCN)(L^2)] (right (2), methylpyridine at N7, X = CH, Y = N). Counterions and hydrogen atoms omitted for clarity. Ref. 35 Copyright (2015) Wiley-VCH Verlag GmbH & Co. KGaA, Weinheim.

N7 bonds longer and flexible than the metal-N3 bonds. This explains well the difference in activation barrier for the two Mn^{IV}=O isomers. The Fe-based oxidants are reacting via σ-pathway, barely dependent on the steric factor of the bispidine ligand, and therefore reactivity has been switched in these cases. The importance of ^4E states in dictating the reactivity differences in these species could not be ruled out as CASSCF/NEVPT2 data are not available.

2.2. *Five-coordinated $Mn^{III/IV}$ = O species*

Unlike *hexa*-coordinated Mn^{IV}=O species, penta-coordinated trigonal–bipyramidal complexes of Mn^{III}=O and Mn^{IV}=O species have different crystal field splitting patterns. In case of Mn^{III}=O species, the four electrons in the five metal d-orbitals are found to have $(\pi^*_{yz})^1$ $(\pi^*_{xz})^1$ $(\delta^*_{x^2-y^2})^1$ $(\delta_{xy})^1$ $(\sigma^*_{z^2})^0$ configuration with nearly degenerate $\pi^*_{yz} = \pi^*_{xz}$ and $\delta^*_{x^2-y^2} = \delta_{xy}$ orbitals. For the Mn^{IV}=O on the other hand, a $(\pi^*_{yz})^1$ $(\pi^*_{xz})^1$ $(\delta^*_{xy})^1(\delta^*_{x^2-y^2})^0$ $(\sigma^*_{z^2})^0$ electronic configuration was detected with the degeneracy between the π^*_{yz} and π^*_{xz} orbitals lifted to some extent (see Fig. 5). The splitting patterns observed for these species are entirely different for the tetragonal complexes. For Mn-complexes in general, the observation of spin-crossover is very rare,[36] due to a small gain in ligand field stabilisation energy, which is outweighed by the energy penalty of pairing two electrons in one orbital. Thus the paring energy associated with the raising of destabilising Coulomb repulsion and drop in exchange energy in stabilising low-spin state contribute to the rare observance of such spin-crossover behaviour in Mn systems. This is in contrast to the Fe^{IV}=O species, where geometry around the metal ion play a proactive role in modulating the spin of the ground state. Several penta-coordinated trigonal bipyramidal $Mn^{III/IV/V}$=O complexes in the $[H_3buea]^{3-}$ ($[H_3buea]^{3-}$ = tris[(*N'-tert-butylureaylato*)-*N*-*ethylene*)]aminato) ligand environment has been reported by the Borovik group over the past few decades. Due to the role of constrained hydrogen bond cavity around the M=O centre, these complexes are of interest and found to be reactive as oxidants.[37]

Although several experimental studies have been documented on these complexes, detailed theoretical studies are very few in this area. Towards this direction, we have recently reported the mechanistic aspect of the formation of Mn^{III}=O and Mn^{IV}=O species in the tetradentate tripodal ligand environment $[H_3buea]^{3-}$ from Mn^{II} precursor complex and O_2 as oxidant using the DFT method.[38] The use of $[H_3buea]^{3-}$ ligand is proven to be strategically very important because of its ability to control the secondary coordination sphere by forming a sterically constrained hydrogen-bonding cage around the metal-oxo/hydroxo moiety, minimising the probability of dimerisation and facilitating the formation of a variety of structurally similar monomeric metal oxo/hydroxo complexes in different oxidation states. Among the various

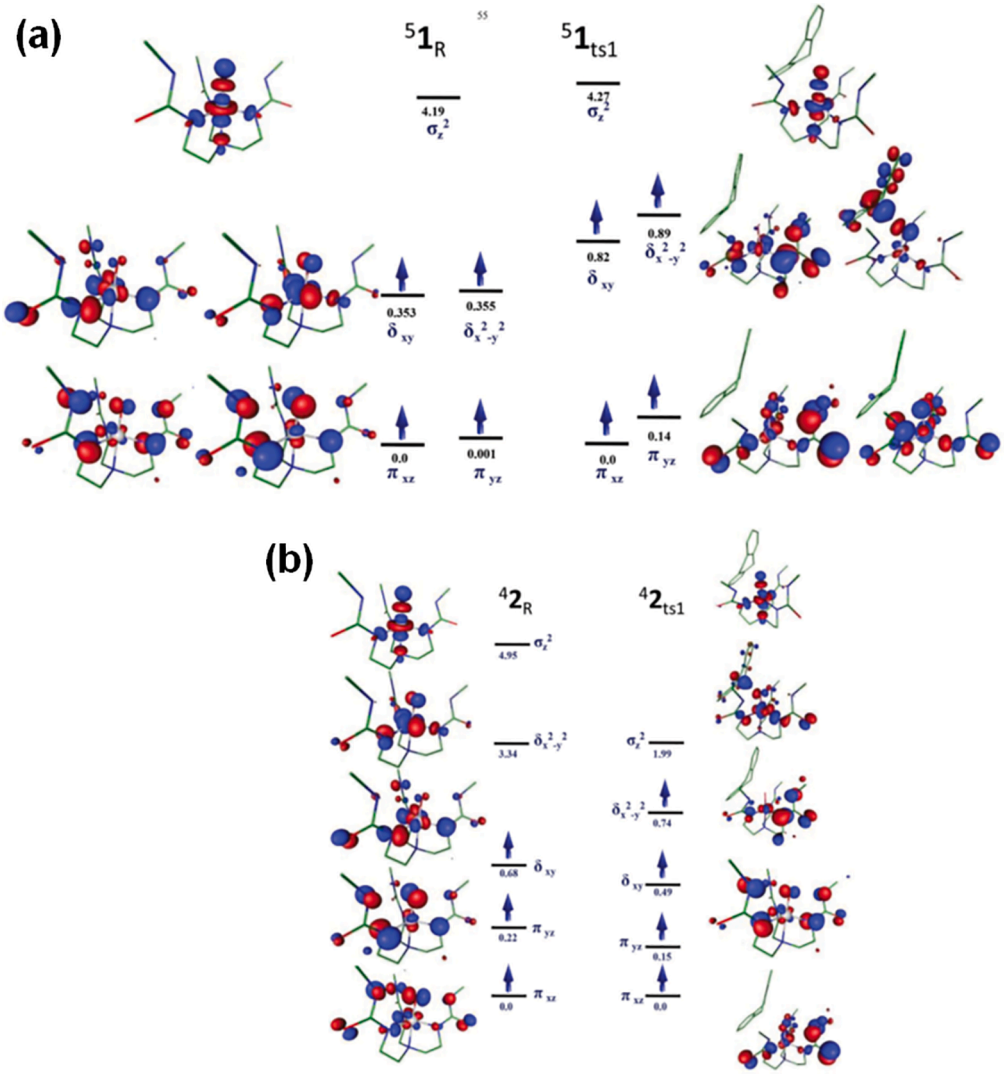

Fig. 5. (a) Relative thermodynamic free energies between $Mn^{III/IV}$ = O and its hydroxo complexes, and (b) The feasible electron shifts between the σ_{C-H} bond and Mn–O d-based orbitals for Mn^{III} = O and Mn^{IV} = O species. Reprinted (adapted) with permission from ref 40. Copyright (2013) The Royal Society of Chemistry.

possible pathways explored, the most facile one includes the formation of Mn^{II}-superoxide species by O_2 activation followed by the formation of Mn^{II}-hydroperoxo species $[Mn^{II}H_2buea(OOH)]^{2-}$. The solvent dimethylacetamide (DMA) itself acts as a proton source for hydrogen atom transfer. In the next step, O—O bond cleavage is taking place, which is found to be aided by the presence of water molecule, resulting $[Mn^{III}H_3buea(O)]^{2-}$ which undergoes one-electron oxidation leading to $[Mn^{IV}H_3buea(O)]^{-}$ species (Scheme 2). Involvement of various spin-states has been shown in this study considering spins on both metal and negatively charged nitrogen atoms (denoted in green in Scheme 2) of one of the urea arms of the $[H_3buea]^{3-}$ ligand, although the overall reaction is facilitated in the high-spin surface. In the present study, a unique multistate reactivity has been proposed where the oxidation state of the metal-ion is unaltered due to the non-innocent nature of the ligand. Moreover, a correlation between the spin states and the hydrogen-bonding interactions has been demonstrated.[39]

Previous experimental work of Borovik and co-workers on the $[(H_3buea)Mn^{III/IV}{=}O]$ species have shown that the terminal oxo-ligand in these species are basic, having the p*K*a values of ~28.3 and ~15, respectively.[12] The large difference in the basicity is directly indicative of the different mechanisms associated with these species, which is in fact also supported by the different reactivity patterns of these species with 2,4,6-tri-*tert*-butylphenol. While the $[(H_3buea)Mn^{III}{=}O]$ species deprotonates the substrate, the oxidative counterpart ends up with the homolytic cleavage of the O—H bond, resulting in phenoxyl radical and $[Mn^{III}(O)H_3buea]^{-}$. Moreover, kinetic analysis with DHA as substrate in DMSO reveals the higher reactivity of $Mn^{III}{=}O$ species than $Mn^{IV}{=}O$, with the rate constant one magnitude larger for the former. Based on these observations, later Jaccob et al. have studied the comparative reactivity as well as the mechanistic aspect of $[Mn^{III}(O)H_3buea]^{2-}$ and $[Mn^{IV}(O)H_3buea]^{2-}$ species towards C—H activation of dihydroanthracene (DHA) using the DFT.[40] The density functional theory approach also supports the higher reactivity of $[Mn^{III}(O)H_3buea]^{2-}$ (54.2 kJ/mol) as compared to its one-electron oxidised counterpart (63.2 kJ/mol) in activating an aliphatic C—H bond. There are earlier reports where the C—H bond activation by the high-valent metal-oxo species is known to take place by multiple possible pathways such as (i) a step-wise proton transfer followed by electron transfer (PT-ET), (ii) a step-wise electron transfer followed by proton transfer (ET-PT) and (iii) a concerted proton-coupled electron transfer (PCET) mechanisms. In this study, the species with higher basicity were found to prefer a proton-transfer electron transfer mechanism for the C—H activation process, while the relatively less basic $[Mn^{IV}(O)H_3buea]^{-}$ species follows a concerted proton-coupled electron transfer (PCET) pathway for the same (Scheme 3). The mechanism has been well rationalised using the schematic MO diagrams of both catalysts $[Mn^{III}(O)H_3buea]^{2-}$/$[Mn^{IV}(O)H_3buea]^{-}$ and the first transition state (Fig. 5). For the $Mn^{III}{=}O$ species, the transfer of spin-up α, as well as spin-down β-electron from the σ_{CH} orbital is not possible as the empty σ_z^2 orbital is strongly destabilised to accept an α-electron. Also, the β-electron transfer is prohibited due to reduction in exchange interactions. These factors are familiar for $Mn^{IV}{=}O$ species, where the electron-accepting $\delta_{x^2-y^2}$ orbital is comparatively low-lying, and also the electron transfer causes the exchange enhancement (Fig. 5). The reactivity difference is mainly attributed to the Mn-O basicity, relative Mn-O bond strength and thermodynamic driving forces during the reaction. As CASSCF/NEVPT2 data were not available, the role of the excited state in facilitating/diminishing the reactivity could not be commented.

Later, we have also reported the reactivity of $[Mn^{IV}(O)H_3buea]^{-}$ catalyst towards oxygen atom transfer using various derivatives of phosphines such as PPh_2Me, $PPhMe_2$, PCy_3, PPh_3, and PMe_3 employing DFT as well as *ab initio* CASSCF/NEVPT2 methods.[41] The $S = {}^3/_2$ state is found to be the ground state dictating the reactivity for all substrates. A state-average CASSSF/NEVPT2 calculation on the $[Mn^{IV}(O)H_3buea]^{-}$ species indicates the presence of multiconfigurational character for these species, which is in agreement with the previous studies. The ground state is found to be strongly admixed with the excited state electronic configurations, the dominating electronic structure $(\delta_{xy})^1(\pi^*_{yz})^1(\pi^*_{xz})^1$ is contributing only 32% to the total wave-function having a strong mixing with the $(\delta_{xy})^1(\pi^*_{xz})^1(\delta^*_{x^2-y^2})^1$ (18%) and $(\delta_{xy})^1(\pi^*_{yz})^1(\sigma^*_{z^2})^1$ (17%) excited states respectively (Fig. 6a). The mixing of the ground state with the excited state is supported by the TD-DFT analysis, where a weak band in the near-IR region (930 nm) corresponding to the $\pi^*_{xz}/\pi^*_{yz} \rightarrow \delta^*_{x^2-y^2}$ transition is found. These unique features in the near-IR regions are also in line with the previous literature.[31] Further, in the reactant complex species, the less contributing excited state configurations dominate over the $(\delta_{xy})^1(\pi^*_{yz})^1(\pi^*_{xz})^1$ configuration. Two reactant complexes have been found, one with the dominant $(\pi^*_{yz})^1(\pi^*_{xz})^1(\delta^*_{x^2-y^2})^1$ (27%) configuration and another with the $(\delta_{xy})^1(\pi^*_{yz})^1(\sigma^*_{z^2})^1$ (38%) configuration. The energy barrier associated with the $\delta_{xy} \rightarrow \delta^*_{x^2-y^2}$ excitation is quite high (83.5 kJ/mol) while the barrier associated with the other $\pi^*_{xz} \rightarrow \delta^*_{z^2}$ is smaller (43.1 kJ/mol). Therefore the latter determines the reaction rate (Fig. 6b). The predicted reactivity pattern is estimated to be PCy_3 (65.5 kJ/mol) < PMe_3 (63.5 kJ/mol) < PPh_3 (63.3 kJ/mol) < $PPhMe_2$ (44.8 kJ/mol) < PPh_2Me (43.1 kJ/mol) which agrees well with the experimental observations. All of the substrates are found to react via a rare δ-pathway where a spin-up α-electron is getting transferred to the $\delta^*_{x^2-y^2}$ orbital. The presence of multireference character points towards the existence of various reaction channels as well as reaction patterns for the molecules having Mn=O moiety with ligand capable of exhibiting secondary coordination sphere.

2.3. *Six-coordinate $Mn^V{=}O$ species*

Unlike $Mn^{IV}{=}O$ species, one electron oxidised non-heme $Mn^V{=}O$ species are not prone towards the above-described excited state reactivity. DFT calculations have been performed only on a very few $Mn^V{=}O$ species so far, and all of them are indicative of the involvement of comparatively simple single-state or two-state reactivity phenomenon. A study on the $[(S\text{-}PMB)Mn^V(O)(OAc)]^{2+}$ reveals that the species is stabilised in the S = 1 surface due to the presence of degenerate low-lying π^*_{xy} and π^*_{yz} orbitals.[34] The abstraction of hydrogen from the cyclohexane occurs without altering the spin state with a moderate energy barrier. The other energy states are found to be very high due to the reduction of exchange enhanced reactivity. A radical mechanism is found to be operated with the Mn—O—H angle of ~120°, resulting in a π-pathway.

Previous reports suggest that the reactive $Mn^n{=}O$ species are better described as $Mn^{(n-1)}$-O• species, and these can be directly related to the proposal that the open-shell radical species are prone to nucleophilic reactions rather than closed-shell systems.[42] Siegbahn and co-workers have proposed that in the Brudvig catalyst, $Mn^V{=}O$ species remains as Mn^{IV}-O• form for facile O—O bond formation. These two species are electromers, and there is a possibility that the two form remains equal.[43] Density functional theory studies with popular functionals on the high-valent $Mn^V{=}O$ species results in the dominating Mn^{IV}-O• species, but these results are found to be extremely dependent on the exchange-correlation functional employed, which leads to uncertainty on the fact that whether the $Mn^V{=}O$ species remains in its conventional form or to its isomeric oxyl radical form. The CASPT2 calculations reveal the existence of the Mn^{IV}-O• form, which is found to be dominating with the hybrid functionals (B3LYP). Further, a relationship is found between the oxidation state of the metal and the spin polarisation and diradical character. It has been concluded that these species can be best described as a structure between two extreme points.

3. Mechanistic insights on high-valent Mn-Nitrene species

The metallonitrene species are analogues to metal-oxo counterparts and participate in various important industrial and biological reactions such as aziridination and C—H bond amination. Among various methods

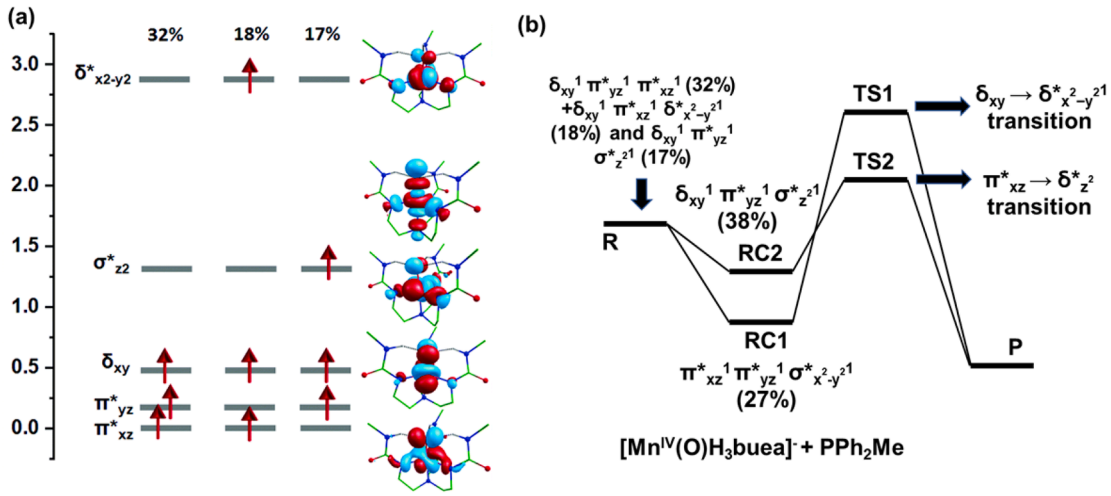

Fig. 6. (a) CASSSFT/NEVPT2 based frontier d-based orbital energies of the S = $^3/_2$ state for $[Mn^{IV}H_3buea(O)]^-$ species. All the energy values are in eV unit. (b) Schematic representation of the involvement of excited states in the reaction of $[Mn^{IV}H_3buea(O)]^-$ with PPh_2Me.Reprinted (adapted) with permission from ref 41. Copyright (2013) The Royal Society of Chemistry.

available for the synthesis of aziridines, direct nitrene transfer to olefins is found to be most viable as it retains stereo and chemoselectivity. Here we aim to summarise various Mn-nitrene species and their reactivities. As studies on Mn-nitrene are very limited, we have covered both heme and non-heme Mn-nitrene species where DFT calculations were employed as a tool to understand the underlying mechanism of C—H and C═C bond activation.

Bagchi *et. al.* have reported a detailed mechanistic study on non-heme $[Mn^{II}(L)(CH_3CN)]^-$ (L = *N,N',N''*-(nitrilotris(benzene-2,1-diyl)) tris(2,2,2-trifluoroacetamide) with styrene and isopentene using experiments and DFT calculations.[44] Here, two-step aziridination takes place; (1) N-C_β bond formation and (2) radical rebound of styrene with metal nitrene active species (see Scheme 4). The activation free energy barrier ($\Delta G^{\#}$) for the initial C_β–N_{Ts} bond-formation step of aziridination was found to be 105.0 kJ/mol for styrene and 137.2 kJ/mol for isopentane. The radical rebound step barrier is reported as 19.7 kJ/mol (styrene) and 14.2 kJ/mol (isopentene). The rate-limiting step in both cases is initial C—N bond formation. Due to the higher energy of HOMO in styrene (0.7 eV) compared to isopentene, the nucleophilic character of styrene is found to be higher than isopentane. Among styrene and isopentene, electrophilic attack of Mn^{IV}=NTs species on styrene is found to have a lower barrier (105.0 kJ/mol). The isopentene rebound step has a small barrier (14.2 kJ/mol) due to the higher reactivity of alkyl radical than benzyl radical intermediate. The variation in the overall thermodynamic of both reactions is very different. In the case of styrene, the reaction is highly exothermic in nature with 203.3 kJ/mol energy, while isopentene reaction is slightly exothermic by 15.1 kJ/mol. This observation indicates that the isopentene aziridination is more difficult than that of styrene, where benzylic radical intermediate is present. While CASSCF/NEVPT2 calculations were proven to be pivotal to the understanding of Mn-oxo reactivity, and such studies were not available on Mn-nitrene to explore the possible excited state reactivities.

The Breslow and coworkers reported the $[Mn^{III}(TFPP)Cl]$ (TFPP = 5,10,15,20-tetrakis(pentafluorophenyl)porphyrinato) complex catalyzed regioselective hydroxylation and amidation of equilenin derivatives with PhI = O and PhI = NTs, respectively.[45] Recently, theoretical studies to understand the mechanistic feature of this reaction has been undertaken by Liyuan et al.[46] Here, different regioselectivity of amidation and hydroxylation are explored. Even though the barrier height for PhI•••X bond cleavage is high in both cases (60.2 kJ/mol for Mn^{III}-OIPh and 80.8 kJ/mol for Mn^{III}-N(Ts)IPh), but in comparing the C(sp^2)-H at C-6 and C(sp^3)-H at the C-11 position of equilenin hydroxylation and amidation, the barrier height differs significantly. The C(sp^2)-H hydroxylation at C-6 position proceeds via oxygen atom transfer (OAT) mechanism with a barrier height of 14.6 kJ/mol, while C(sp^3)-H amidation at C-11 takes place with hydrogen atom abstraction (HAA) mechanism with a barrier height of 21.3 kJ/mol (Scheme 5). The reason for the OAT mechanism for hydroxylation is that Mn-oxo is electron-deficient which facilitate the electrophilic addition to the aromatic ring. On the other hand, the nitrogen atom transfer (NAT) at the C-6 position is not feasible due to the less electronegativity of nitrogen compared to oxygen and the large steric effect of the bulky NTs group. The hydroxylation OAT and HAA [C(sp^3)-H at C-11] energy difference is only 6.7 kJ/mol, while the energy difference in amidation of NAT and HAA [C(sp^3)-H at C-11] is 20.5 kJ/mol. This observation is consistent with the experimental results of major hydroxylation products at the C-6 position and single amidation products at the C-11 position.

White and co-workers[26] reported a novel manganese catalyst $[Mn^{III}(^{tBu}Pc)]^+$ (^{tBu}Pc = *tert*-butylphthalocyanine) which shows high chemoselectivity with high reactivity for allylic substrate (*E*)-hex-4-en-1-yl sulfamate. Recently, Zhan and coworkers[47] performed the DFT studies to unravel the factors behind the high reactivity and high chemoselectivity. Here, they have considered porphyrazine (Pz) instead of ^{tBu}Pc to reduce the computational cost. The mechanistic studies suggest that the C—H amination barrier for HAA is 22.6 kJ/mol while the C═C aziridination barrier for nitrogen attack is 64.0 kJ/mol (see Scheme 5). This indicates that the C—H amination product is preferred over C═C aziridination, which is consistent with the experimental product ratio of amination product to aziridination product (>20:1). The C—H amination is favourable both kinetically and thermodynamically compared to C═C aziridination. The radicals generated after the HAA in C—H amination are stabilised by the alkene π bond, and a seven-membered ring during the HAA transition state is less strained compared to an eight-membered ring in C═C aziridination (see Scheme 6). The chemoselectivity between C—H and C═C originated from the structure rigidity and planar nature of Pz ligand, which results in a large steric repulsion between Pz and sulfamate substrate moieties in the aziridination. All these factors indicate that C—H amination is preferred over C═C aziridination. The higher reactivity of $[Mn^{III}Pz]^+$ complex is due to the nature of the Pz ligand, which contains four stronger electronegative N atoms (see Scheme 6). This increases the ability of the Pz ligand to accept electrons compared to the porphyrin ligand.

Recently, White and coworkers[25] developed a perchloroinated manganese phthalocyanine complex $[Mn^{III}(ClPc)SbF_6]$ (ClPc = chlorinated phtalocyanine) which shows benzylic C(sp^3)-H reactivity over the tertiary C(sp^3)-H bond (see Scheme 7). The mechanistic studies have

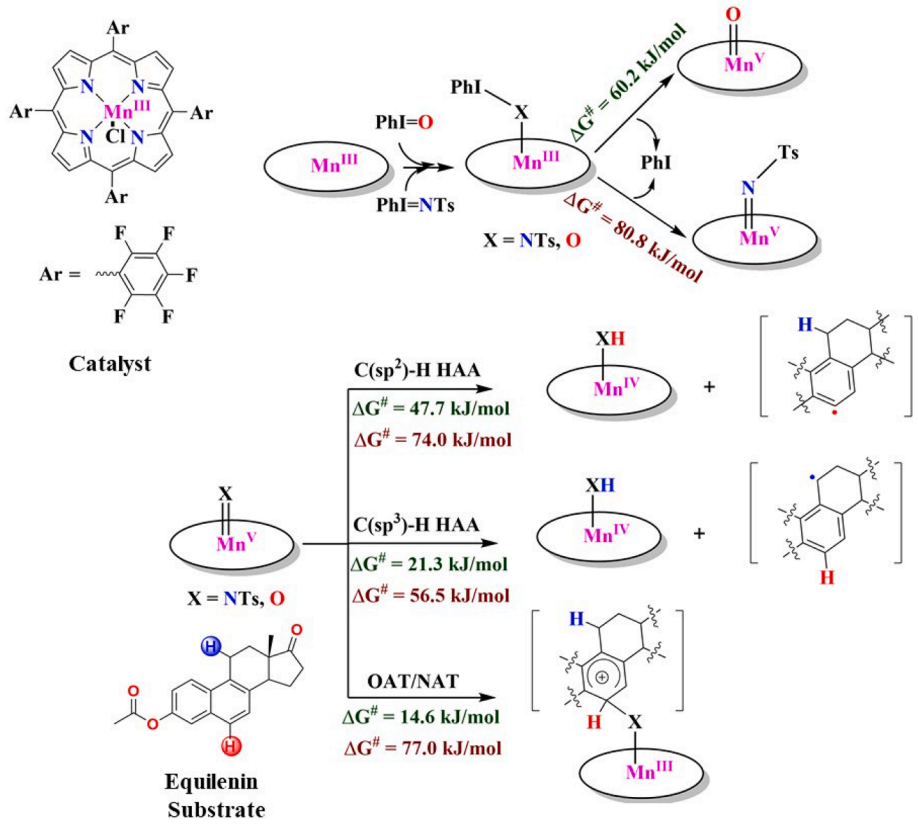

(a)

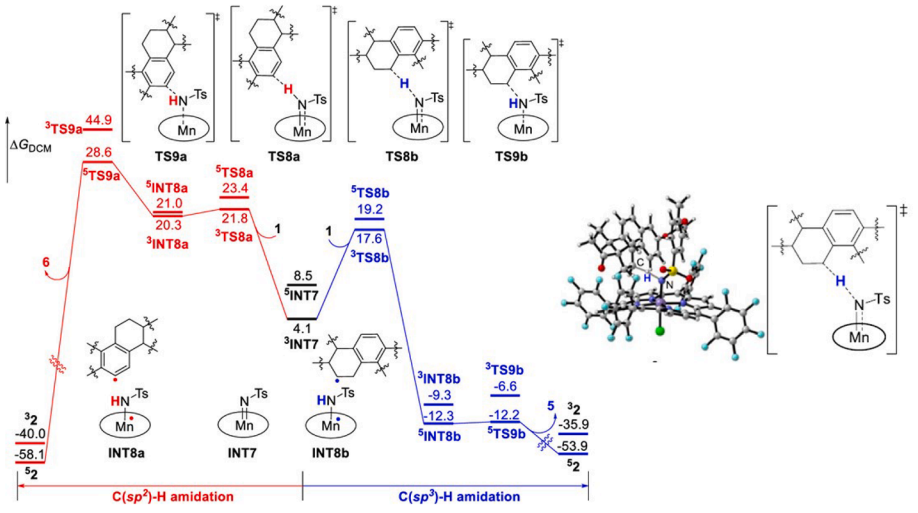

(b)

Scheme 5. (a) Schematic representation of various pathways involved in the reaction with their activation barriers ($\Delta G^{\#}$) in kJ/mol and (b) Energy Profile diagram (kcal/mol) and optimised geometry of lower transition state where C—H, N—H bond lengths and Mn—N—H angle are 1.31 Å, 1.39 Å and 117.0° from ref. 46 Copyright (2020) American Chemical Society.

been performed by Wang and co-workers.[48] Here, they have verified that SbF_6^- acts as a spectator ion in complex $[Mn^{III}(ClPc)SbF_6]$ and performed the studies using $[Mn^{III}(ClPc)]^+$. The nitrogen source used here is PhI = NTces ($TcesNH_2$ = 2,2,2-trichloroethyl sulfamate). As discussed previously, here also the barrier height for PhI removal is high for the reactive species generation (42.7 kJ/mol) (Scheme 7). That is a reasonable barrier at the reaction temperature

of 40 °C. The C—H bond activation at the benzylic position takes place through hydride atom transfer (HYT) instead of HAA. The reason for the HYT mechanism is the non-innocent redox-active nature of the ClPc ligand in $[Mn^{III}(ClPc)]^+$ complex. During the Mn-nitrene formation, the ClPc loses one electron to form a radical cation on the ClPc moiety. Then, ClPc radical cation accepts an electron from the C—H bond. A cationic species at the benzylic position is generated on the substrate after HYT. The observed fact from this mechanism is that the metal oxidation state will not change during this process. In summary,

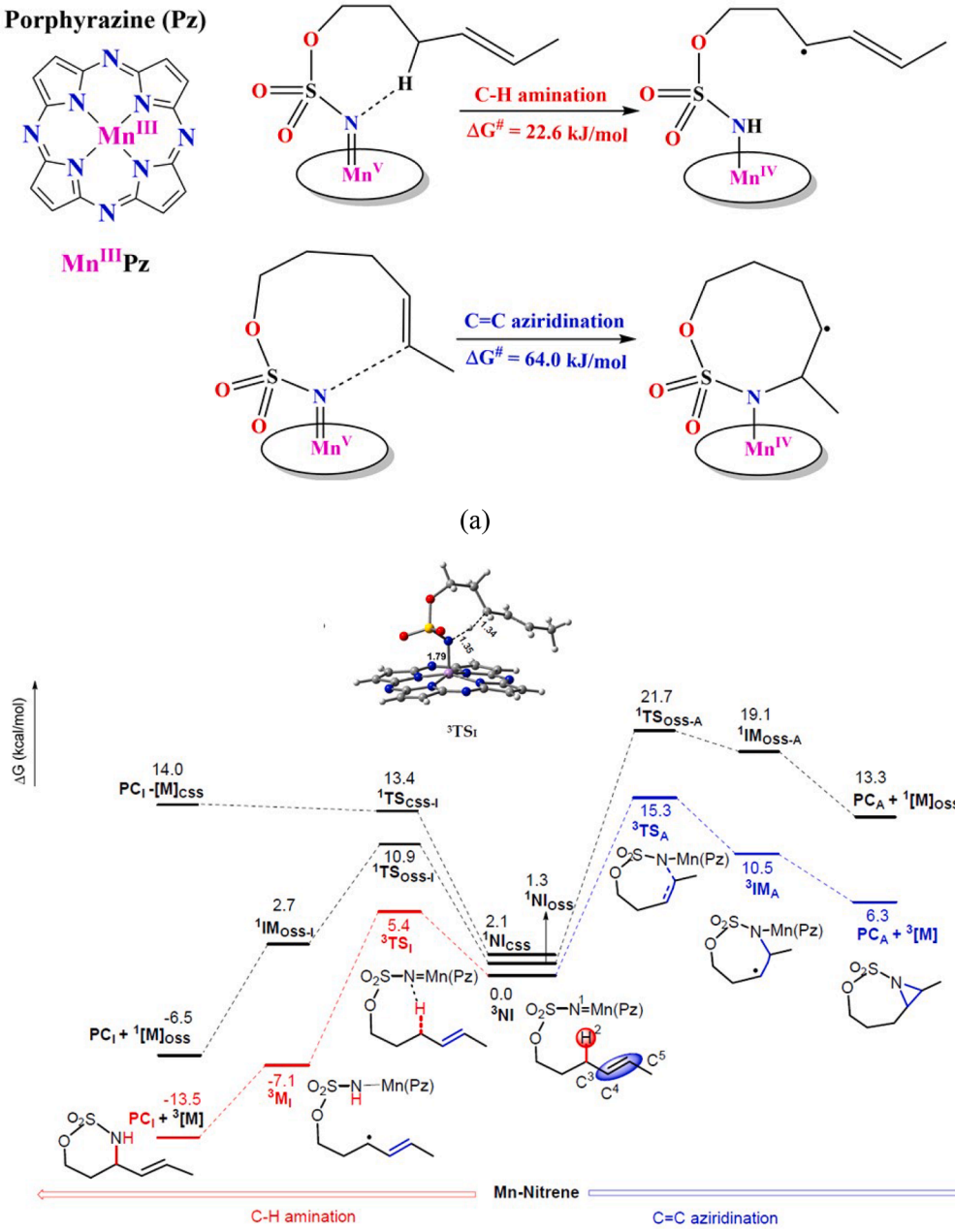

Scheme 6. (a) Schematic representation of various pathways involved in the reaction with their activation barriers (ΔG#) in kJ/mol (b) the energy profile diagram (kcal/mol) along with optimised geometry of lower transition states from ref. [47].

the Mn-nitrene species follows the different pathways based on the attached ligand architecture and nitrogen donor substrate. As we have seen, that HYT pathway is followed by highly electron-deficient $[Mn^{III}(ClPc)]^{+}$ moiety while the other two reviewed moieties $[Mn^{III}(TFPP)Cl]$ and $[Mn^{III}Pz]^{+}$ follow the HAA pathway during C—H activation. The regioselectivity and chemoselectivity of these complexes are highly appreciated to make pharmaceutical drugs.

4. Conclusions

In the present minireview, we have focused on theoretical studies devoted in understanding the intriguing reactivity observed for various mononuclear high-valent Mn-oxo/nitrene species towards C—H and C=C bond activation to draw a parallel to the popular Fe^{IV}=O chemistry. Unlike Fe^{IV}=O/NTs chemistry, where the concept of two-state reactivity with excited high-spin state dominating the rate-limiting step, in Mn-O/NTs chemistry, the high-spin states are generally the ground state and hence are the only state participating in the reactivity – much like a single state reactivity (SSR) concept with a twist. The twist is the participation of d-electronic excited states of the same multiplicity in reactivity in the Mn-oxo chemistry. These states were often too high in energy in Fe^{IV}=O species and hence are not accessible to participate in the reactivity. This reactivity pertains only to Mn^{IV}=O species so far, while $Mn^{III/V}$=O species reported following single-state reactivity based on S = 2/S = 1 ground state. For the Mn^{IV}=O species, the $S = {}^{3}/_{2}$ is found to be the ground state, which remains unaltered throughout the reaction. In the presence of substrate, another d-electronic excited $S = {}^{3}/_{2}$ state (^{4}E) becomes accessible, triggering the reactivity. The transition state corresponding to the ^{4}E state is found to be the rate-determining in many oxidative reactions studied, unveiling the importance of this state in controlling the reactivity of Mn^{IV}=O species. Although the computed barriers heights are hard to compare due to some difference in the

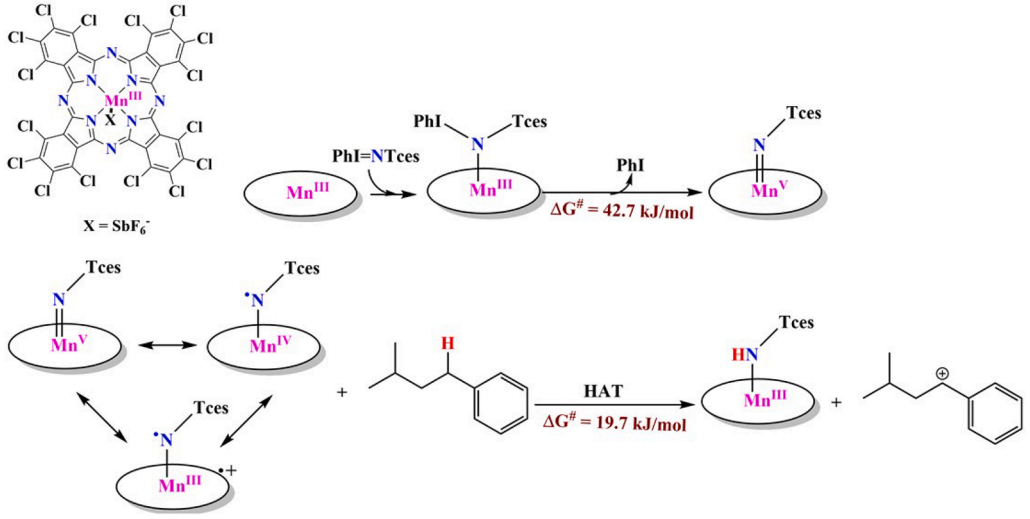

(a)

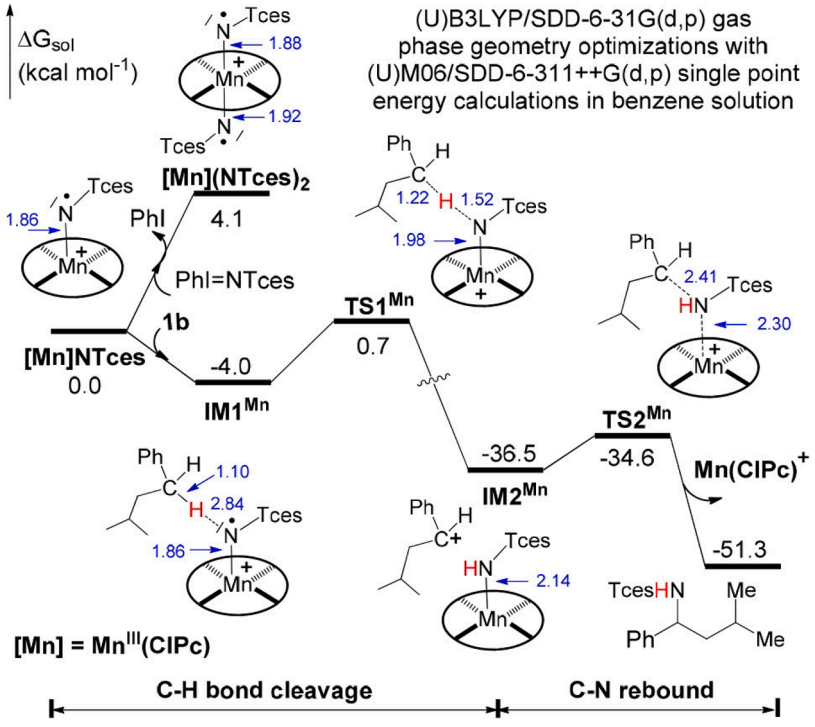

(b)

Scheme 7. (a) Schematic representation of various pathways involved in the reaction with their activation barriers ($\Delta G^{\#}$) in kJ/mol and (b) the Gibbs free energy (in kcal/mol) profile diagram for the reaction of [Mn]NTces^{+} from ref. 48 Copyright (2020) American Chemical Society.

methodology employed, the computed barrier height for the C—H bond activation provide qualitatively the following order of decreasing reactivity $[Mn^{IV}(O)(BnTPEN)]^{2+}$ > $[Mn^{IV}(O)(N4py)]^{2+}$ > $[Mn^{IV}(O)L^{2}]^{2+}$ > $[Mn^{IV}(O)(OH)(Me_2EBC)]^{+}$ > $[Mn^{IV}(O)(H_3buea)]^{-}$. Among these complexes studied $[Mn^{IV}(O)(BnTPEN)]^{2+}$ is found to be the most reactive, and this may be attributed to the smaller ^4B-^4E gap increasing the radical character on the oxyl oxygen atoms. It is clear that lower energy between the two excited states should be targeted to obtain a better catalyst. In order to reduce the ^4B-^4E gap, the following factors can be considered, (i) modulating the ligand architecture, (ii) modulating the donor atoms, particularly weaker donor atoms expected to stabilise the excited states (iii) geometry around the metal centre (iv) secondary coordination sphere and (v) presence of Lewis acid around the oxyl oxygen atom. There are several examples in the literature which lacks theoretical studies but shows different reactivity that is attributed difference in the ligand architecture.[49] Additionally, as excited states play a proactive role in the oxidation catalysis of Mn-oxo species, accessing these states photochemically is likely to open up new frontiers. DFT calculations on the Mn-nitrene species towards C═C azirdination and C—H bond amination barrier places $[Mn^{V}(ClPc)(NTces)(SbF_6)]$ to be the most reactive with a very small kinetic barrier while $[Mn^{IV}(NTs)(L)(CH_3CN)]^{-}$ (L = *N,N',N''*-(nitrilotris(benzene-2,1-diyl))tris(2,2,2-trifluoroacetamide) is found to the least reactive. Although the role of excited states in dictating the reactivities was not explored for the Mn-nitrene species, a fraction of the barrier found for the heme analogue compared to the non-heme analogue indicate that such intricate excited

states which are likely to be stabilised with heme type ligand system could play a role in the reactivity of these species as well.

Declaration of Competing Interest

The authors declare that they have no known competing financial interests or personal relationships that could have appeared to influence the work reported in this paper.

Acknowledgement

We thank DST and SERB (CRG/2018/00430; DST/CSA-03/2018-10; SB/SJF/2019-20/12) for funding. AS thanks CSIR for a fellowship and RK for SRF fellowship.

References:

[1] W.B. Tolman, Activation of Small Molecules: Organometallic and Bioinorganic Perspectives, John Wiley & Sons, 2006.
[2] D. Schröder, S. Shaik, H. Schwarz, Acc. Chem. Res. 33 (2000) 139–145.
[3] R. Kumar, A. Ansari, G. Rajaraman, Chem. Eur. J. 24 (2018) 6818–6827.
[4] R. Kumar, B. Pandey, G. Rajaraman, J. Indian Chem. Soc 96 (2019) 825–836.
[5] S. Shaik, H. Chen, D. Janardanan, Nat. Chem. 3 (2011) 19–27.
[6] R. Kumar, B. Pandey, A. Sen, M. Ansari, S. Sharma, G. Rajaraman, Coord. Chem. Rev. 419 (2020), 213397.
[7] D. Janardanan, Y. Wang, P. Schyman, L. Que Jr, S. Shaik, Angew. Chem. 122 (2010) 3414–3417.
[8] D. Usharani, D. Janardanan, C. Li, S. Shaik, Acc. Chem. Res. 46 (2013) 471–482.
[9] X. Wu, M.S. Seo, K.M. Davis, Y.-M. Lee, J. Chen, K.-B. Cho, Y.N. Pushkar, W. Nam, J. Am. Chem. Soc. 133 (2011) 20088–20091.
[10] A.A. Massie, A. Sinha, J.D. Parham, E. Nordlander, T.A. Jackson, Inorg. Chem. 57 (2018) 8253–8263.
[11] J. Chen, Y.-M. Lee, K.M. Davis, X. Wu, M.S. Seo, K.-B. Cho, H. Yoon, Y.J. Park, S. Fukuzumi, Y.N. Pushkar, J. Am. Chem. Soc. 135 (2013) 6388–6391.
[12] T.H. Parsell, M.-Y. Yang, A. Borovik, J. Am. Chem. Soc. 131 (2009) 2762–2763.
[13] A. Borovik, Chem. Soc. Rev. 40 (2011) 1870–1874.
[14] R. Kumar, B. Pandey, A. Singh, G. Rajaraman, Inorg. Chem. 60 (2021) 12085–12099.
[15] B. Meunier, S.P. De Visser, S. Shaik, Chem. Rev. 104 (2004) 3947–3980.
[16] S. Shaik, D. Kumar, S.P. de Visser, A. Altun, W. Thiel, Chem. Rev. 105 (2005) 2279–2328.
[17] K.-B. Cho, H. Hirao, S. Shaik, W. Nam, Chem. Soc. Rev. 45 (2016) 1197–1210.
[18] A.K. Vardhaman, P. Barman, S. Kumar, C.V. Sastri, D. Kumar, V.S.P. de, Angew. Chem., Int. Ed. 52 (2013) 12288–12292.
[19] B. Pandey, M. Jaccob, G. Rajaraman, Chem. Commun. 53 (2017) 3193–3196.
[20] Y. Park, Y. Kim, S. Chang, Chem. Rev. 117 (2017) 9247–9301.
[21] L. Degennaro, P. Trinchera, R. Luisi, Chem. Rev. 114 (2014) 7881–7929.
[22] P. Heretsch, S. Rabe, A. Giannis, J. Am. Chem. Soc. 132 (2010) 9968–9969.
[23] A.I. Lazar, F. Biedermann, K.R. Mustafina, K.I. Assaf, A. Hennig, W.M. Nau, J. Am. Chem. Soc. 138 (2016) 13022–13029.
[24] W. Kaplan, H.R. Khatri, P. Nagorny, J. Am. Chem. Soc. 138 (2016) 7194–7198.
[25] J.R. Clark, K. Feng, A. Sookezian, M.C. White, Nat. Chem. 10 (2018) 583–591.
[26] S.M. Paradine, J.R. Griffin, J. Zhao, A.L. Petronico, S.M. Miller, M.C. White, Nat. Chem. 7 (2015) 987.
[27] C.-M. Che, V.K.-Y. Lo, C.-Y. Zhou, J.-S. Huang, Chem. Soc. Rev. 40 (2011) 1950–1975.
[28] H. Lu, X.P. Zhang, Chem. Soc. Rev. 40 (2011) 1899–1909.
[29] K.-B. Cho, S. Shaik, W. Nam, J. Phys. Chem. Lett. 3 (2012) 2851–2856.
[30] J. Chen, A. Draksharapu, E. Harvey, W. Rasheed, L. Que, W.R. Browne, Chem. Commun. 53 (2017) 12357–12360.
[31] D.F. Leto, A.A. Massie, D.B. Rice, T.A. Jackson, J. Am. Chem. Soc. 138 (2016) 15413–15424.
[32] D.B. Rice, A.A. Massie, T.A. Jackson, Inorg. Chem. 58 (2019) 13902–13916.
[33] J. Chen, K.-B. Cho, Y.-M. Lee, Y.H. Kwon, W. Nam, Chem. Commun. 51 (2015) 13094–13097.
[34] X.-X. Li, M. Guo, B. Qiu, K.-B. Cho, W. Sun, W. Nam, Inorg. Chem. 58 (2019) 14842–14852.
[35] P. Barman, A.K. Vardhaman, B. Martin, S.J. Wörner, C.V. Sastri, P. Comba, Angew. Chem. 127 (2015) 2123–2127.
[36] S. Amabilino, R.J. Deeth, Inorg. Chem. 56 (2017) 2602–2613.
[37] S.A. Cook, A. Borovik, Acc. Chem. Res. 48 (2015) 2407–2414.
[38] A. Sen, N. Vyas, B. Pandey, M. Jaccob, G. Rajaraman, Isr. J. Chem. 60 (2020) 973–986.
[39] B. Pandey, A. Ansari, N. Vyas, G. Rajaraman, J. Chem. Sci. 127 (2015) 343–352.
[40] M. Jaccob, A. Ansari, B. Pandey, G. Rajaraman, Dalton Trans. 42 (2013) 16518–16526.
[41] A. Sen, N. Vyas, B. Pandey, G. Rajaraman, Dalton Trans. 49 (2020) 10380–10393.
[42] D.C. Ashley, M.-H. Baik, ACS Catal. 6 (2016) 7202–7216.
[43] M. Lundberg, M.R. Blomberg, P.E. Siegbahn, Inorg. Chem. 43 (2004) 264–274.
[44] V. Bagchi, A. Kalra, P. Das, P. Paraskevopoulou, S. Gorla, L. Ai, Q. Wang, S. Mohapatra, A. Choudhury, Z. Sun, ACS Catal. 8 (2018) 9183–9206.
[45] J. Yang, R. Weinberg, R. Breslow, Chem. Commun. (2000) 531–532.
[46] L. Jin, Q. Wang, X. Chen, N. Liu, X. Fang, Y.-F. Yang, Y.-B. She, J. Org. Chem. 85 (2020) 14879–14889.
[47] J. Wang, K. Zheng, T. Li, X. Zhan, Catalysts 10 (2020) 292.
[48] Z. Liu, Y. Lu, J. Guo, W. Hu, Y. Dang, Z.-X. Wang, Org. Lett. 22 (2020) 453–457.
[49] M. Sankaralingama, M. Palaniandavar, Dalton Trans. 43 (2014) 538–550.